Earth Syst. Dynam. Discuss., 6, 1605–1633, 2015
www.earth-syst-dynam-discuss.net/6/1605/2015/
doi:10.5194/esdd-6-1605-2015

Earth System Dynamics
Discussions
Open Access

The eigenvalue problem for ice-shelf vibrations: comparison of a full 3-D model with the thin plate approximation

Y. V. Konovalov

Department of Mathematics, National Research Nuclear University MEPhI, Kashirskoe Shosse, 31, 115409, Moscow, Russia

Received: 16 August 2015 – Accepted: 19 August 2015 – Published: 7 September 2015

Correspondence to: Y. V. Konovalov (yu-v-k@yandex.ru)

Published by Copernicus Publications on behalf of the European Geosciences Union.

Abstract

Ice-shelf forced vibration modelling is performed using a full 3-D finite-difference elastic model, which also takes into account sub-ice seawater flow. The ocean flow in the cavity is described by the wave equation; therefore, ice-shelf flexures result from hydrostatic pressure perturbations in sub-ice seawater layer. Numerical experiments have been carried out for idealized rectangular and trapezoidal ice-shelf geometries. The ice-plate vibrations are modelled for harmonic ingoing pressure perturbations and for high-frequency spectra of the ocean swells. The spectra show distinct resonance peaks, which demonstrate the ability to model a resonant-like motion in the suitable conditions of forcing. The spectra and ice-shelf deformations obtained by the developed full 3-D model are compared with the spectra and the deformations modelled by the thin-plate Holdsworth and Glynn model (1978). The main resonance peaks and ice-shelf deformations in the corresponding modes, derived by the full 3-D model, are in agreement with the peaks and deformations obtained by the Holdsworth and Glynn model. The relative deviation between the eigenvalues (periodicities) in the two compared models is about 10 %. In addition, the full model allows observation of 3-D effects, for instance, the vertical distribution of the stress components in the plate. In particular, the full model reveals an increase in shear stress, which is neglected in the thin-plate approximation, from the terminus towards the grounding zone with a maximum at the grounding line in the case of the considered high-frequency forcing. Thus, the high-frequency forcing can reinforce the tidal impact on the ice-shelf grounding zone causing an ice fracture therein.

1 Introduction

Tides and ocean swells produce ice-shelf bends and, thus, they can initiate break-up of ice in the marginal zone (Holdsworth and Glynn, 1978; Goodman et al., 1980; Wadhams, 1986; Squire et al., 1995; Meylan et al., 1997; Turcotte and Schubert, 2002)

ESDD
6, 1605–1633, 2015

and also excite ice-shelf rift propagation. No strong correlation between rift propagation rate and ocean swell impact have been revealed so far (Bassis et.al., 2008), and it is not clear to what degree the rift propagation can potentially be triggered by tides and ocean swells. Nevertheless, the impact of tides and ocean swells is a fraction of the total force (Bassis et al., 2008) that produces ice calving in ice shelves (MacAyeal et al., 2006). Moreover, a resonant-like motion in suitable conditions of long-term swell forcing (several periods of the swell impact) can cause a fracture in the ice-shelf (Holdsworth and Glynn, 1978). Thus, new knowledge on the vibration process in ice shelves is important for the investigation of ice-sheet–ocean interactions and sea level change due to alterations in the ice calving rate.

Several models of ice-shelf bends and ice-shelf vibrations have been proposed by several researchers, e.g. Holdsworth (1977), Hughes (1977), Holdsworth and Glynn (1978), Goodman et al. (1980), Lingle et al. (1981), Wadhams (1986), Smith (1991), Vaughan (1995), Schmeltz et al. (2001), Turcotte and Schubert (2002), on the basis of elastic thin plate/elastic beam approximations. These models allow simulations of ice-shelf deformations, calculate the bending stresses emerging due to the processes of vibrations, and assess possible effects of tides and ocean swell impacts on the calving process. Further development of elastic-beam models for description of ice-shelf flexures implies application of viscoelastic rheological models. In particular, tidal flexures of ice-shelf are obtained using the linear viscoelastic Burgers model by Reeh et al. (2003) and Walker et al. (2013), and using the nonlinear 3-D viscoelastic full Stokes model by Rosier et al. (2014).

Ice-stream response to ocean tides has been described by full Stokes 2-D finite-element employing a non-linear viscoelastic Maxwell rheological model by Gudmundsson (2011). This model revealed that tidally induced ice-stream motion is strongly sensitive to the parameters of the sliding law. In particular, a non-linear sliding law allows for the explanation of an ice stream response to ocean forcing at long-tidal periods (MSf) through a nonlinear interaction between the main semi-diurnal tidal components (Gudmundsson, 2011).

ESDD
6, 1605–1633, 2015

A 2-D finite-element flow-line model with an elastic rheology was developed by O. V. Sergienko (Bromirski et al., 2010; Sergienko, 2010), and was used to estimate mechanical impact of a high-frequency tidal action on the stress regime of ice shelves. In this model (Sergienko, 2010), seawater was considered as an incompressible, inviscid fluid, and was described by the velocity potential.

In this work, the modelling of forced vibrations of a buoyant, uniform, elastic ice-shelf, floating in shallow water of variable depth, was developed. The simulations of the bends of the ice-shelf were performed by a full 3-D finite-difference elastic model. The main objectives of the study were as follows: firstly, to introduce a method that provides stability to the numerical solution in the full finite-difference elastic model based on the coupling of the fundamental momentum equations with the wave equation for the water layer; secondly, to compare the results – the amplitude spectra and the ice-shelve deformations – obtained by the full 3-D model developed here with the spectra and the deformations modelled by the thin-plate Holdsworth and Glynn model (1978) (Appendix A) with the intention of revealing the principal distinctions, if any, and specifications of the full model.

2 Field equations

2.1 Basic equations

The 3-D elastic model is based on well-known momentum equations (e.g. Lamb, 1994; Landau and Lifshitz, 1986):

$$\begin{cases} \dfrac{\partial \sigma_{xx}}{\partial x} + \dfrac{\partial \sigma_{xy}}{\partial y} + \dfrac{\partial \sigma_{xz}}{\partial z} = \rho \dfrac{\partial^2 U}{\partial t^2}; \\ \dfrac{\partial \sigma_{yx}}{\partial x} + \dfrac{\partial \sigma_{yy}}{\partial y} + \dfrac{\partial \sigma_{yz}}{\partial z} = \rho \dfrac{\partial^2 V}{\partial t^2}; \\ \dfrac{\partial \sigma_{zx}}{\partial x} + \dfrac{\partial \sigma_{zy}}{\partial y} + \dfrac{\partial \sigma_{zz}}{\partial z} = \rho \dfrac{\partial^2 W}{\partial t^2}; \\ 0 < x < L; y_1(x) < y < y_2(x); h_b(x,y) < z < h_s(x,y), \end{cases} \tag{1}$$

ESDD
6, 1605–1633, 2015

where (xyz) is a rectangular coordinate system with the x axis along the central line, and the z axis is pointing vertically upward; U, V and W are two horizontal and one vertical ice displacements, respectively; σ is the stress tensor; ρ is ice density; $h_b(xy)$ and $h_s(xy)$ are ice bed and ice surface elevations, respectively; L is the glacier length along the central line; and $y_1(x)$, $y_2(x)$ are the lateral edges. In a normal condition of arbitrary ice-shelf geometry, it is assumed that the x axis direction is chosen so that the lateral edges can be approximated by single-value functions $(y_1(x), y_2(x))$.

The sub-ice water is considered as an incompressible non-viscous fluid of uniform density. Another assumption is that the water depth changes gradually horizontally. Under these assumptions, the sub-ice water flows uniformly in a vertical column, and the manipulation with the continuity equation and the Euler equation yields the wave equation (Holdsworth and Glynn, 1978)

$$\frac{\partial^2 W_b}{\partial t^2} = \frac{1}{\rho_w}\frac{\partial}{\partial x}\left(d_0\frac{\partial P'}{\partial x}\right) + \frac{1}{\rho_w}\frac{\partial}{\partial y}\left(d_0\frac{\partial P'}{\partial y}\right), \tag{2}$$

where ρ_w is sea water density; $d_0(xy)$ is the depth of the sub-ice water layer; $W_b(xyt)$ is the ice-shelf base vertical deformation, and $W_b(x,y,t) = W(xyh_bt)$; $P'(xyt)$ is the deviation from the hydrostatic pressure.

For harmonic vibrations, the method of separation of variables yields the same equations, in which only the operator $\frac{\partial^2}{\partial t^2}$ needs to be replaced with $-\omega^2$, where ω is the frequency of the vibrations for xyz-dependent values. Likewise, the deformation due to the gravitational forcing is excluded in the vibration problem, i.e. the term ρg as well as the appropriate terms in the boundary conditions listed below are absent in the final equations formulated for the vibration problem.

2.2 Boundary conditions

The boundary conditions are (i) stress free ice surface, (ii) normal stress exerted by seawater at the ice-shelf free edges and at the ice-shelf base, and (iii) rigidly fixed edge at the origin of the ice-shelf (i.e. in the glacier along the grounding line). In detail, the well-known form of the boundary conditions, for example, at the ice-shelf base is expressed as

$$\begin{cases} \sigma_{xz} = \sigma_{xx}\frac{\partial h_\mathrm{b}}{\partial x} + \sigma_{xy}\frac{\partial h_\mathrm{b}}{\partial y} + P\frac{\partial h_\mathrm{b}}{\partial x}; \\ \sigma_{yz} = \sigma_{yx}\frac{\partial h_\mathrm{b}}{\partial x} + \sigma_{yy}\frac{\partial h_\mathrm{b}}{\partial y} + P\frac{\partial h_\mathrm{b}}{\partial y}; \\ \sigma_{zz} = \sigma_{zx}\frac{\partial h_\mathrm{b}}{\partial x} + \sigma_{zy}\frac{\partial h_\mathrm{b}}{\partial y} - P, \end{cases} \tag{3}$$

where P is pressure ($P = \rho g H + P'$, H is ice-shelf thickness).

In this developed model, we considered an approach where the known boundary conditions (Eq. 3) were incorporated into the basic Eq. (1). A suitable form of the equations can be written after discretization of the model (Konovalov, 2012), which is shown below.

In the ice-shelf forced vibration problem, the boundary conditions for the water layer are as follows: (i) at the boundaries coinciding with the lateral free edges: $\frac{\partial P'}{\partial \boldsymbol{n}} = 0$, where $\boldsymbol{n}$ is the unit horizontal vector normal to the edges; (ii) at the boundary along the grounding line: $\frac{\partial P'}{\partial \boldsymbol{n}} = 0$, where $\boldsymbol{n}$ is the unit horizontal vector normal to the grounding line; and (iii) at the ice-shelf terminus the pressure perturbations are excited by the periodical impact of the ocean wave: $P' = P'_0 \sin \omega t$.

2.3 Discretization of the model

Numerical solutions are obtained with a finite-difference method, which is based on the standard coordinate transformation $xyz \to x$, $\eta = \frac{y-y_1}{y_2-y_1}$, $\xi = (h_\mathrm{s} - z)/H$. The coordinate transformation transfigures an arbitrary ice domain into the rectangular parallelepiped $\Pi = \{0 \le x \le L; 0 \le \eta \le 1; 0 \le \xi \le 1\}$.

Numerical experiments with ice flow models and with elastic models (Konovalov, 2012, 2014) have shown that the method, in which the initial boundary conditions Eq. (3) are included in the momentum Eq. (1), can be applied in the finite-difference models. In certain cases, this approach additionally provides numerical stability to the solution. In this work, the method has been applied in the developed 3-D elastic model. The procedure for this inclusion is described in Appendix B.

2.4 Equations for ice-shelf displacements

Constitutive relationships between stress tensor components and displacements correspond to Hook's law (e.g. Landau and Lifshitz, 1986; Lurie, 2005):

$$\sigma_{ij} = \frac{E}{1+\nu}\left(u_{ij} + \frac{\nu}{1-2\nu}u_{ll}\delta_{ij}\right), \tag{4}$$

where u_{ij} represents the strain components.

Substitution of these relationships into Eq. (1), and Eqs. (B1)–(B5) gives the final equations of the model.

3 Results of the numerical experiments

3.1 Amplitude spectra and deformations

The numerical experiments with ice-shelf forced vibrations were carried out for a physically idealized ice plate having rectangular and trapezoidal profiles (Fig. 1). The three experiments that differ in ice-shelf/cavity geometries as shown in Fig. 1 are considered here. A difference in the spectra obtained from among the three experiments implied an impact of the cavity geometry and of the ice-shelf geometry on the eigenfrequencies of the shelf–water system.

In Experiment A, ice-shelf thickness and the water layer depth were kept constant (Fig. 1a).

In Experiment B, an expanding water layer was considered (Fig. 1b). The expanding water layer is in agreement with the observations (e.g. Holdsworth and Glynn, 1978)

ESDD
6, 1605–1633, 2015

and leads to the change in the spreading velocity of a long gravity wave in the channel (due to changes in d_0). Therefore, the cavity geometry change should yield changes in the eigenfrequencies and, thus, it reflects the impact of the cavity geometry on the eigenfrequencies of the shelf–water system.

In addition, in Experiment C, a tapering ice-shelf was considered (Fig. 1, c). As in the case of the expanding cavity, firstly, the tapering ice-shelf is in agreement with the observations (e.g. Holdsworth and Glynn, 1978). Secondly, the taper of the ice-shelf should yield changes in the eigenfrequencies of the shelf–water system due to a change in the average ice-plate thickness.

Figures 2–4 show the amplitude spectra obtained for all the three experiments. The amplitude spectrum, shown in Fig. 2, is split into parts for a better visualization of the resonance peaks in the spectrum.

Figures 5 and 6 show the ice-shelf deformations that responded to the eigenfrequencies derived from the amplitude spectra in Experiment A and C, respectively.

3.1.1 Experiment A

The first four eigenvalues can be distinguished easily in the spectra shown in Fig. 2. They are approximately equal to 37.1, 14.2, 7.1, and 4.21 s in the full model and are approximately equal to 41.1, 14, 6.7, and 3.81 s, respectively, in the Holdsworth and Glynn model. The maximum difference between the eigenvalues is observed for the first eigenvalue, which corresponds to the largest peak in the spectra in Fig. 2a. The relative deviation for the first four eigenvalues varies from 2 to 10 %. The deformations obtained by the two models are in agreement in the spatial distributions of nodes/antinodes (Fig. 5).

3.1.2 Experiment B

This experiment reveals the same trend in the difference between the eigenvalues obtained from both considered models (Fig. 3). Specifically, as in Experiment A, the max-

ESDD

6, 1605–1633, 2015

The eigenvalue problem for ice-shelf vibrations

Y. V. Konovalov

imum difference between the eigenvalues is observed for the first eigenvalue. The first three eigenvalues are approximately equal to 43.2, 16.8, and 8.4 s in the full model and are approximately equal to 48.3, 16.5, and 7.9 s, respectively, in the Holdsworth and Glynn model. The maximum relative deviation is also equal to about 11 %. Moreover, Experiment B justified the eigenvalue dependence on the cavity geometry in both considered models. The deviation for the eigenvalues due to the cavity geometry changes is about 17 % (Table 1).

3.1.3 Experiment C

There are no new particulars (in comparison with previous experiments) in the relative position of the resonance peaks obtained from the considered models (Fig. 4) in Experiment C. The first four eigenvalues are approximately equal to 66.9, 21.2, 10.3, and 5.9 s in the full model and are approximately equal to 68.8, 20.5, 9.8, and 5.5 s, respectively, in the Holdsworth and Glynn model. The maximum relative deviation for the tapering ice-shelf is smaller in comparison with the previous values (in Experiment A and B) and is about 3–7 %. Experiment C in comparison with Experiment B similarly shows that the ice-shelf geometry change (average ice-shelf thickness increase/decrease) also yields shifts in the resonance peaks. The relative deviation due to the ice-shelf geometry change is about 37 to 57 %. As in Experiment A, for coinciding (corresponding) eigenvalues the deformations in the modes are in agreement for the two considered models (Fig. 6).

3.2 Shear stress distribution in the vertical cross-section

Figure 7 shows shear stress distributions in the vertical cross-section along the centre line. Obtained distributions reveal that the maximum shear stress is next to the grounding line. For instance, in Experiment A, near-resonance forcing, which corresponds to the second eigenvalue (Fig. 5b), induces a threshold value of 10^6 Pa in the maximum, when the amplitude of the incident wave becomes about 0.5 m. Hence, we can assume

ESDD
6, 1605–1633, 2015

that long-term forcing can cause fracture in this ice-shelf, which is considered in Experiment A. Moreover, we can obtain such stress distributions for any ice-shelf geometry and for any resonance peak to estimate risks of the impact of the near-resonance incident waves.

4 Summary

The ice-shelf forced vibration modelling can be performed by the 3-D full elastic model, although the volume of the routine sufficiently increases in comparison with the thin-plate model.

The numerical experiments have shown the impact of shelf/cavity geometry on the amplitude spectrum. The alterations of the geometries excite shifts in the peak positions. Therefore, the prediction ability for resonant-like ice-shelf motion is dependent on (i) detailed ice-shelf surface/base topography (ii) detailed numbers and positions of the crevasses, and (iii) detailed seafloor topography under the ice-shelf.

The complementary shear stress, which can be derived in the full model, in the case of high-frequency forced vibrations, are an order of magnitude less in the maximum than the maximal value of the component σ_{xx}. Thus, in general, the analysis of shear stress justifies application of the thin plate theory in the case of high-frequency vibrations, when ice displacements are relatively small. Nevertheless, the results evidently maintain the fact that shear stress should reinforce dislocations in the nodes (of the mode), where shear stress reaches the local maxima/minima (Fig. 7). Furthermore, the 3-D model reveals that the maximum of the shear stress is next to the grounding line (at the fixed edge of the plate), thus the high-frequency vibrations can reinforce the tidal impact in the grounding zone.

In the forced vibration problem, in which the dissipative factors are neglected, amplitudes in the peaks (Fig. 2), in general, are undefined (unlimited). A realistic finite motion in the peaks can be modelled by considering the limitation of the ingoing overall water flux in the model, which is based on the original equations for the water layer (continuity

ESDD
6, 1605–1633, 2015

equation and Euler equation). This model includes applicable boundary conditions for ingoing water flux and, hence, yields specific amplitude spectra with limited amplitudes in resonance peaks (Konovalov, 2014).

Thus, the full 3-D model yields quantitatively similar results, which were obtained by a model based on thin-plate approximation (Holdsworth and Glynn, 1978). The maximum relative deviation for the eigenvalues in the test experiments does not exceed 11 % and the maximum is observed for the first eigenvalue. This can be explained by the assessment of the first eigenfrequency, which is obtained considering the thin-plate approximation. The assessment is expressed as

$$\omega_0 \approx \alpha \sqrt{\frac{E}{\left(1-\nu^2\right)\rho_{\mathrm{w}} L^2}} \sqrt{\frac{d_0 H}{L^2}} \frac{H}{L}. \tag{5}$$

Therefore, considering $d_0 \sim H \ll L$, the assessment (Eq. 5) includes a second power of the small parameter $\gamma \sim \sqrt{\frac{d_0 H}{L^2}}$. Thus, taking into account that essentially the first eigenfrequency is an expansion in powers of the small parameter, we can evaluate the relative deviation for the eigenvalue. The next term of the expansion contains the third (or higher) power of the small parameter. Therefore, the relative deviation includes the first power of the small parameter, i.e. in the experiments is estimated as $\gamma \sim 5\,\%$.

Appendix A: Field equations of the thin-plate model (Holdsworth and Glynn model)

Holdsworth and Glynn forced vibration model (1978), which is considered in the test experiments (A, B and C) as the basic model, includes the following equations.

Thin-plate vibration equation (the momentum equation) is

$$\frac{\partial^2 M_x}{\partial x^2} + \frac{\partial^2 M_y}{\partial y^2} - 2\frac{\partial^2 M_{xy}}{\partial x \, \partial y} = \rho H \frac{\partial^2 W}{\partial t^2} + \rho_{\mathrm{w}} g W - P', \tag{A1}$$

ESDD
6, 1605–1633, 2015

The eigenvalue problem for ice-shelf vibrations

Y. V. Konovalov

where $W(xyt)$ is vertical deformation; ρ is ice density; H is ice-shelf thickness; ρ_w is seawater density; g is the acceleration of gravity; P' is the deviation from the hydrostatic pressure; M_x, M_y and M_{xy} are bending moments to lateral loading and they are expressed as

$$M_x = -D\left(\frac{\partial^2 W}{\partial x^2} + \nu \frac{\partial^2 W}{\partial y^2}\right), \tag{A2}$$

$$M_y = -D\left(\frac{\partial^2 W}{\partial y^2} + \nu \frac{\partial^2 W}{\partial x^2}\right), \tag{A3}$$

$$M_{xy} = D\,(1-\nu)\,\frac{\partial^2 W}{\partial x\,\partial y}, \tag{A4}$$

where D is flexural rigidity: $D = \frac{E H^3}{12\left(1-\nu^2\right)}$.

The wave equation for water layer is

$$\frac{\partial^2 W}{\partial t^2} = \frac{1}{\rho_w}\frac{\partial}{\partial x}\left(d_0 \frac{\partial P'}{\partial x}\right) + \frac{1}{\rho_w}\frac{\partial}{\partial y}\left(d_0 \frac{\partial P'}{\partial y}\right), \tag{A5}$$

where $d_0(xy)$ is the depth of the sub-ice water layer.

The boundary conditions are as follows:

1. At $x = 0$ (fixed boundary): $W = 0$; $\frac{\partial W}{\partial x} = 0$; $M_x = \frac{1}{\nu} M_y$; $M_{xy} = 0$; $\frac{\partial P'}{\partial x} = 0$.
2. At $x = L_x$ (ice-shelf terminus): $M_x = 0$; $M_y = D\,\frac{1-\nu^2}{\nu}\,\frac{\partial^2 W}{\partial x^2}$; $\frac{\partial M_x}{\partial x} = 2\,\frac{\partial M_{xy}}{\partial y}$; $M_{xy} = D\,(1-\nu)\,\frac{\partial^2 W}{\partial x\,\partial y}$; $P' = A\rho_w g \sin \omega t$; where A is the amplitude of the incident wave, ω is the frequency of the forcing (incident wave).
3. At $x = 0$, $x = L_y$ (lateral edges of the ice-shelf): $M_y = 0$; $M_x = D\,\frac{1-\nu^2}{\nu}\,\frac{\partial^2 W}{\partial y^2}$; $\frac{\partial M_y}{\partial y} = 2\,\frac{\partial M_{xy}}{\partial x}$; $M_{xy} = D\,(1-\nu)\,\frac{\partial^2 W}{\partial x\,\partial y}$; $\frac{\partial P'}{\partial y} = 0$.

Appendix B: Boundary conditions employed in the full model

In this work, the method, in which the initial boundary conditions Eq. (3) are included in the momentum Eq. (1), is employed with intent to obtain the stable numerical solution in the full finite-difference model. The procedure for this inclusion consists of the following successive steps:

1. We rewrite, for instance, the first equation from Eq. (1) using the new variables:

$$\frac{\partial \sigma_{xx}}{\partial x} + \eta'_x \frac{\partial \sigma_{xx}}{\partial \eta} + \xi'_x \frac{\partial \sigma_{xx}}{\partial \xi} + \eta'_y \frac{\partial \sigma_{xy}}{\partial \eta} + \xi'_y \frac{\partial \sigma_{xy}}{\partial \xi} + {\xi'}_z \frac{\partial \sigma_{xz}}{\partial \xi} = \rho \frac{\partial^2 U}{\partial t^2}.$$

2. We write the approximation of the derivative $\frac{\partial \sigma_{xz}}{\partial \xi}$ at the ice-shelf base towards the substance (glacier):

$$\left({\xi'}_z \frac{\partial \sigma_{xz}}{\partial \xi}\right)^{N_\xi} = -\frac{1}{H}\left(\frac{\partial \sigma_{xz}}{\partial \xi}\right)^{N_\xi} \approx -\frac{1}{H}\frac{1}{2\,\Delta\xi}\sigma_{xz}^{N_\xi-2} + \frac{1}{H}\frac{4}{2\,\Delta\xi}\sigma_{xz}^{N_\xi-1} - \frac{1}{H}\frac{3}{2\,\Delta\xi}\sigma_{xz}^{N_\xi};$$

   where index N_ξ corresponds to grid layer located at the ice-shelf base.

3. The standard (typical) boundary conditions at the ice-shelf base Eq. (3) require that $\sigma_{xz} = \sigma_{xx}\frac{\partial h_b}{\partial x} + \sigma_{xy}\frac{\partial h_b}{\partial y} + P\frac{\partial h_b}{\partial x}$. Thus, we should replace $\sigma_{xz}^{N_\xi}$ in agreement with the standard boundary conditions, with $\left\{\sigma_{xx}\frac{\partial h_b}{\partial x} + \sigma_{xy}\frac{\partial h_b}{\partial y}\right\}^{N_\xi} + P\frac{\partial h_b}{\partial x}$. Finally, we obtain the following approximation of the derivative $\left({\xi'}_z \frac{\partial \sigma_{xz}}{\partial \xi}\right)^{N_\xi}$ at the ice-shelf base:

$$\left(\xi'_z \frac{\partial \sigma_{xz}}{\partial \xi}\right)^{N_\xi} \approx -\frac{1}{H}\frac{1}{2\,\Delta\xi}\sigma_{xz}^{N_\xi-2} + \frac{1}{H}\frac{4}{2\,\Delta\xi}\sigma_{xz}^{N_\xi-1} - \frac{1}{H}\frac{3}{2\,\Delta\xi}\left\{\sigma_{xx}\frac{\partial h_\mathrm{b}}{\partial x} + \sigma_{xy}\frac{\partial h_\mathrm{b}}{\partial y}\right\}^{N_\xi}$$
$$-\frac{1}{H}\frac{3}{2\,\Delta\xi}P'\frac{\partial h_\mathrm{b}}{\partial x} - \frac{3}{2\,\Delta\xi}\rho g\frac{\partial h_\mathrm{b}}{\partial x},$$

where $P = \rho g H + P'$.

4. Thus, at the ice-shelf base, we apply the equation

$$\left(\frac{\partial \sigma_{xx}}{\partial x}\right)^{N_\xi} + \left(\eta'_x \frac{\partial \sigma_{xx}}{\partial \eta}\right)^{N_\xi} + \left(\xi'_x \frac{\partial \sigma_{xx}}{\partial \xi}\right)^{N_\xi} + \left(\eta'_y \frac{\partial \sigma_{xy}}{\partial \eta}\right)^{N_\xi} + \left(\xi'_y \frac{\partial \sigma_{xy}}{\partial \xi}\right)^{N_\xi}$$
$$-\frac{1}{H}\frac{1}{2\,\Delta\xi}\sigma_{xz}^{N_\xi-2} + \frac{1}{H}\frac{4}{2\,\Delta\xi}\sigma_{xz}^{N_\xi-1} - \frac{1}{H}\frac{3}{2\,\Delta\xi}\left\{\sigma_{xx}\frac{\partial h_\mathrm{b}}{\partial x} + \sigma_{xy}\frac{\partial h_\mathrm{b}}{\partial y}\right\}^{N_\xi} - \frac{1}{H}\frac{3}{2\,\Delta\xi}P'\frac{\partial h_\mathrm{b}}{\partial x}$$
$$\approx \frac{3}{2\,\Delta\xi}\rho g\frac{\partial h_\mathrm{b}}{\partial x} + \rho\left(\frac{\partial^2 U}{\partial t^2}\right)^{N_\xi},$$

which is the first equation at the ice-shelf base, instead of the standard equation $\sigma_{xz} = \sigma_{xx}\frac{\partial h_\mathrm{b}}{\partial x} + \sigma_{xy}\frac{\partial h_\mathrm{b}}{\partial y} + P\frac{\partial h_\mathrm{b}}{\partial x}$.

Therefore, after the coordinate transformation, the applicable equations at ice-shelf base can be written as

$$\begin{cases} \left(\frac{\partial \sigma_{xx}}{\partial x}\right)^{N_\xi} + \left(\eta'_x \frac{\partial \sigma_{xx}}{\partial \eta}\right)^{N_\xi} + \left(\xi'_x \frac{\partial \sigma_{xx}}{\partial \xi}\right)^{N_\xi} + \left(\eta'_y \frac{\partial \sigma_{xy}}{\partial \eta}\right)^{N_\xi} + \left(\xi'_y \frac{\partial \sigma_{xy}}{\partial \xi}\right)^{N_\xi} - \frac{1}{H}\frac{1}{2\Delta\xi}\sigma_{xz}^{N_\xi-2} + \\ \frac{1}{H}\frac{4}{2\Delta\xi}\sigma_{xz}^{N_\xi-1} - \frac{1}{H}\frac{3}{2\Delta\xi}\left\{\sigma_{xx}\frac{\partial h_\mathrm{b}}{\partial x} + \sigma_{xy}\frac{\partial h_\mathrm{b}}{\partial y}\right\}^{N_\xi} - \frac{1}{H}\frac{3}{2\Delta\xi}P'\frac{\partial h_\mathrm{b}}{\partial x} \approx \frac{3}{2\Delta\xi}\rho g\frac{\partial h_\mathrm{b}}{\partial x} + \rho\left(\frac{\partial^2 U}{\partial t^2}\right)^{N_\xi}; \\ \\ \left(\frac{\partial \sigma_{yx}}{\partial x}\right)^{N_\xi} + \left(\eta'_x \frac{\partial \sigma_{yx}}{\partial \eta}\right)^{N_\xi} + \left(\xi'_x \frac{\partial \sigma_{yx}}{\partial \xi}\right)^{N_\xi} + \left(\eta'_y \frac{\partial \sigma_{yy}}{\partial \eta}\right)^{N_\xi} + \left(\xi'_y \frac{\partial \sigma_{yy}}{\partial \xi}\right)^{N_\xi} - \frac{1}{H}\frac{1}{2\Delta\xi}\sigma_{yz}^{N_\xi-2} + \\ \frac{1}{H}\frac{4}{2\Delta\xi}\sigma_{yz}^{N_\xi-1} - \frac{1}{H}\frac{3}{2\Delta\xi}\left\{\sigma_{yx}\frac{\partial h_\mathrm{b}}{\partial x} + \sigma_{yy}\frac{\partial h_\mathrm{b}}{\partial y}\right\}^{N_\xi} - \frac{1}{H}\frac{3}{2\Delta\xi}P'\frac{\partial h_\mathrm{b}}{\partial y} \approx \frac{3}{2\Delta\xi}\rho g\frac{\partial h_\mathrm{b}}{\partial y} + \rho\left(\frac{\partial^2 V}{\partial t^2}\right)^{N_\xi}; \\ \\ \left(\frac{\partial \sigma_{zx}}{\partial x}\right)^{N_\xi} + \left(\eta'_x \frac{\partial \sigma_{zx}}{\partial \eta}\right)^{N_\xi} + \left(\xi'_x \frac{\partial \sigma_{zx}}{\partial \xi}\right)^{N_\xi} + \left(\eta'_y \frac{\partial \sigma_{zy}}{\partial \eta}\right)^{N_\xi} + \left(\xi'_y \frac{\partial \sigma_{zy}}{\partial \xi}\right)^{N_\xi} - \frac{1}{H}\frac{1}{2\Delta\xi}\sigma_{zz}^{N_\xi-2} + \\ \frac{1}{H}\frac{4}{2\Delta\xi}\sigma_{zz}^{N_\xi-1} - \frac{1}{H}\frac{3}{2\Delta\xi}\left\{\sigma_{zx}\frac{\partial h_\mathrm{b}}{\partial x} + \sigma_{zy}\frac{\partial h_\mathrm{b}}{\partial y}\right\}^{N_\xi} + \frac{1}{H}\frac{3}{2\Delta\xi}P' \approx -\frac{3}{2\Delta\xi}\rho g + \rho g + \rho\left(\frac{\partial^2 W}{\partial t^2}\right)^{N_\xi}. \end{cases} \tag{B1}$$

ESDD
6, 1605–1633, 2015

The eigenvalue problem for ice-shelf vibrations

Y. V. Konovalov

The same method yields the similar equations at the ice surface

$$\begin{cases} \left(\frac{\partial\sigma_{xx}}{\partial x}\right)^1 + \left(\eta'_x \frac{\partial\sigma_{xx}}{\partial\eta}\right)^1 + \left(\xi'_x \frac{\partial\sigma_{xx}}{\partial\xi}\right)^1 + \left(\eta'_y \frac{\partial\sigma_{xy}}{\partial\eta}\right)^1 + \left(\xi'_y \frac{\partial\sigma_{xy}}{\partial\xi}\right)^1 + \\ \frac{1}{H}\frac{3}{2\,\Delta\xi}\left\{\sigma_{xx}\frac{\partial h_s}{\partial x} + \sigma_{xy}\frac{\partial h_s}{\partial y}\right\}^1 - \frac{1}{H}\frac{4}{2\,\Delta\xi}\sigma^2_{xz} + \frac{1}{H}\frac{1}{2\,\Delta\xi}\sigma^3_{xz} \approx \rho\left(\frac{\partial^2 U}{\partial t^2}\right)^1; \\ \left(\frac{\partial\sigma_{yx}}{\partial x}\right)^1 + \left(\eta'_x \frac{\partial\sigma_{yx}}{\partial\eta}\right)^1 + \left(\xi'_x \frac{\partial\sigma_{yx}}{\partial\xi}\right)^1 + \left(\eta'_y \frac{\partial\sigma_{yy}}{\partial\eta}\right)^1 + \left(\xi'_y \frac{\partial\sigma_{yy}}{\partial\xi}\right)^1 + \\ \frac{1}{H}\frac{3}{2\,\Delta\xi}\left\{\sigma_{yx}\frac{\partial h_s}{\partial x} + \sigma_{yy}\frac{\partial h_s}{\partial y}\right\}^1 - \frac{1}{H}\frac{4}{2\,\Delta\xi}\sigma^2_{yz} + \frac{1}{H}\frac{1}{2\,\Delta\xi}\sigma^3_{yz} \approx \rho\left(\frac{\partial^2 V}{\partial t^2}\right)^1; \\ \left(\frac{\partial\sigma_{zx}}{\partial x}\right)^1 + \left(\eta'_x \frac{\partial\sigma_{zx}}{\partial\eta}\right)^1 + \left(\xi'_x \frac{\partial\sigma_{zx}}{\partial\xi}\right)^1 + \left(\eta'_y \frac{\partial\sigma_{zy}}{\partial\eta}\right)^1 + \left(\xi'_y \frac{\partial\sigma_{zy}}{\partial\xi}\right)^1 + \\ \frac{1}{H}\frac{3}{2\,\Delta\xi}\left\{\sigma_{zx}\frac{\partial h_s}{\partial x} + \sigma_{zy}\frac{\partial h_s}{\partial y}\right\}^1 - \frac{1}{H}\frac{4}{2\,\Delta\xi}\sigma^2_{zz} + \frac{1}{H}\frac{1}{2\,\Delta\xi}\sigma^3_{zz} \approx \rho g + \rho\left(\frac{\partial^2 W}{\partial t^2}\right)^1, \end{cases} \tag{B2}$$

where the upper indices 1–3 in Eq. (B2) denote respectively the numbers of the grid layers starting from the ice surface and moving downward in the vertical direction.

ESDD
6, 1605–1633, 2015

The eigenvalue problem for ice-shelf vibrations

Y. V. Konovalov

Finally, the same manipulations lead to the following equations at the free edges:

a. At $x = L$:

$$\begin{cases} \frac{1}{2\,\Delta x}\sigma_{xx}^{N_x-2} - \frac{4}{2\,\Delta x}\sigma_{xx}^{N_x-1} \approx -\frac{3}{2\,\Delta x} f(\xi) - \left(\xi'_x\right)^{N_x} \frac{\partial f(\xi)}{\partial \xi} + \rho\left(\frac{\partial^2 U}{\partial t^2}\right)^{N_x}; \\ \frac{1}{2\,\Delta x}\sigma_{yx}^{N_x-2} - \frac{4}{2\,\Delta \xi}\sigma_{yx}^{N_x-1} + \left(\eta'_y \frac{\partial \sigma_{yy}}{\partial \eta}\right)^{N_x} + \left(\xi'_y \frac{\partial \sigma_{yy}}{\partial \xi}\right)^{N_x} + \left(\xi'_z \frac{\partial \sigma_{yz}}{\partial \xi}\right)^{N_x} \approx \rho\left(\frac{\partial^2 V}{\partial t^2}\right)^{N_x}; \\ \frac{1}{2\,\Delta x}\sigma_{zx}^{N_x-2} - \frac{4}{2\,\Delta \xi}\sigma_{zx}^{N_x-1} + \left(\eta'_y \frac{\partial \sigma_{zy}}{\partial \eta}\right)^{N_x} + \left(\xi'_y \frac{\partial \sigma_{zy}}{\partial \xi}\right)^{N_x} + \left(\xi'_z \frac{\partial \sigma_{zz}}{\partial \xi}\right)^{N_x} \\ \approx \rho g + \rho\left(\frac{\partial^2 W}{\partial t^2}\right)^{N_x}, \end{cases} \tag{B3}$$

where $f(\xi) = \begin{cases} 0, \ \xi < \frac{h_s}{H}; \\ \rho_w g\,(h_s - \xi H), \ \xi \geq \frac{h_s}{H}. \end{cases}$

ESDD
6, 1605–1633, 2015

The eigenvalue problem for ice-shelf vibrations

Y. V. Konovalov

b. At $y = y_1(x)$:

$$\begin{cases} \left(\frac{\partial\sigma_{xx}}{\partial x}\right)^1 + \left(\eta'_x \frac{\partial\sigma_{xx}}{\partial\eta}\right)^1 + \left(\xi'_x \frac{\partial\sigma_{xx}}{\partial\xi}\right)^1 - \left(\eta'_y\right)^1 \frac{1}{2\,\Delta\eta}\sigma^3_{xy} + \left(\eta'_y\right)^1 \frac{4}{2\,\Delta\eta}\sigma^2_{xy} - \\ \left(\eta'_y\right)^1 \frac{3}{2\,\Delta\eta}\sigma^1_{xx}\frac{\mathrm{d}y_1}{\mathrm{d}x} + \left(\xi'_y \frac{\partial\sigma_{xx}}{\partial\xi}\right)^1 \frac{\mathrm{d}y_1}{\mathrm{d}x} + \left(\xi'_z \frac{\partial\sigma_{xz}}{\partial\xi}\right)^1 \approx \\ \approx -\left(\eta'_y\right)^1 \frac{3}{2\,\Delta\eta} f_x(\xi) + \left(\xi'_y\right)^1 \frac{\mathrm{d}f_x}{\mathrm{d}\xi} + \rho\left(\frac{\partial^2 U}{\partial t^2}\right)^1; \\ \\ \left(\frac{\partial\sigma_{yx}}{\partial x}\right)^1 + \left(\eta'_x \frac{\partial\sigma_{yx}}{\partial\eta}\right)^1 + \left(\xi'_x \frac{\partial\sigma_{yx}}{\partial\xi}\right)^1 - \left(\eta'_y\right)^1 \frac{1}{2\,\Delta\eta}\sigma^3_{yy} + \left(\eta'_y\right)^1 \frac{4}{2\,\Delta\eta}\sigma^2_{yy} - \\ \left(\eta'_y\right)^1 \frac{3}{2\,\Delta\eta}\sigma^1_{yx}\frac{\mathrm{d}y_1}{\mathrm{d}x} + \left(\xi'_y \frac{\partial\sigma_{yx}}{\partial\xi}\right)^1 \frac{\mathrm{d}y_1}{\mathrm{d}x} + \left(\xi'_z \frac{\partial\sigma_{yz}}{\partial\xi}\right)^1 \approx \\ \approx -\left(\eta'_y\right)^1 \frac{3}{2\,\Delta\eta} f_y(\xi) + \left(\xi'_y\right)^1 \frac{\mathrm{d}f_y}{\mathrm{d}\xi} + \rho\left(\frac{\partial^2 V}{\partial t^2}\right)^1; \\ \\ \left(\frac{\partial\sigma_{zx}}{\partial x}\right)^1 + \left(\eta'_x \frac{\partial\sigma_{zx}}{\partial\eta}\right)^1 + \left(\xi'_x \frac{\partial\sigma_{zx}}{\partial\xi}\right)^1 - \left(\eta'_y\right)^1 \frac{1}{2\,\Delta\eta}\sigma^3_{zy} + \left(\eta'_y\right)^1 \frac{4}{2\,\Delta\eta}\sigma^2_{zy} - \\ \left(\eta'_y\right)^1 \frac{3}{2\,\Delta\eta}\sigma^1_{zx}\frac{\mathrm{d}y_1}{\mathrm{d}x} + \left(\xi'_y \frac{\partial\sigma_{zx}}{\partial\xi}\right)^1 \frac{\mathrm{d}y_1}{\mathrm{d}x} + \left(\xi'_z \frac{\partial\sigma_{zz}}{\partial\xi}\right)^1 \approx \rho g + \rho\left(\frac{\partial^2 W}{\partial t^2}\right)^1, \end{cases} \tag{B4}$$

where the upper indices 1–3 in Eq. (B4) denote respectively the numbers of the grid layers starting from the ice lateral edge $y = y_1(x)$, moving in the horizontal transverse direction in the glacier; and

$$f_x = \begin{cases} 0, \ \xi < \frac{h_\mathrm{s}}{H}; \\ \rho_\mathrm{w} g\left(h_\mathrm{s} - \xi H\right)\frac{\mathrm{d}y_1}{\mathrm{d}x}, \ \xi \geq \frac{h_\mathrm{s}}{H}. \end{cases} \quad f_y = \begin{cases} 0, \ \xi < \frac{h_\mathrm{s}}{H}; \\ -\rho_\mathrm{w} g\left(h_\mathrm{s} - \xi H\right), \ \xi \geq \frac{h_\mathrm{s}}{H}. \end{cases}$$

Discussion Paper | Discussion Paper | Discussion Paper | Discussion Paper

ESDD
6, 1605–1633, 2015

c. At $y = y_2(x)$:

$$\begin{cases} \left(\frac{\partial \sigma_{xx}}{\partial x}\right)^{N_\eta} + \left(\eta'_x \frac{\partial \sigma_{xx}}{\partial \eta}\right)^{N_\eta} + \left(\xi'_x \frac{\partial \sigma_{xx}}{\partial \xi}\right)^{N_\eta} + \left(\eta'_y\right)^{N_\eta} \frac{1}{2\,\Delta\eta} \sigma_{xy}^{N_\eta-2} - \\ \left(\eta'_y\right)^{N_\eta} \frac{4}{2\,\Delta\eta} \sigma_{xy}^{N_\eta-1} + \left(\eta'_y\right)^{1} \frac{3}{2\,\Delta\eta} \sigma_{xx}^{N_\eta} \frac{\mathrm{d}y_2}{\mathrm{d}x} + \left(\xi'_y \frac{\partial \sigma_{xx}}{\partial \xi}\right)^{N_\eta} \frac{\mathrm{d}y_2}{\mathrm{d}x} + \left(\xi'_z \frac{\partial \sigma_{xz}}{\partial \xi}\right)^{N_\eta} \approx \\ -\left(\eta'_y\right)^{N_\eta} \frac{3}{2\,\Delta\eta} f_x(\xi) - \left(\xi'_y\right)^{N_\eta} \frac{\mathrm{d}f_x}{\mathrm{d}\xi} + \rho \left(\frac{\partial^2 U}{\partial t^2}\right)^{N_\eta}; \\ \\ \left(\frac{\partial \sigma_{yx}}{\partial x}\right)^{N_\eta} + \left(\eta'_x \frac{\partial \sigma_{yx}}{\partial \eta}\right)^{N_\eta} + \left(\xi'_x \frac{\partial \sigma_{yx}}{\partial \xi}\right)^{N_\eta} + \left(\eta'_y\right)^{N_\eta} \frac{1}{2\,\Delta\eta} \sigma_{yy}^{N_\eta-2} - \\ \left(\eta'_y\right)^{N_\eta} \frac{4}{2\,\Delta\eta} \sigma_{yy}^{N_\eta-1} + \left(\eta'_y\right)^{N_\eta} \frac{3}{2\,\Delta\eta} \sigma_{yx}^{N_\eta} \frac{\mathrm{d}y_2}{\mathrm{d}x} + \left(\xi'_y \frac{\partial \sigma_{yx}}{\partial \xi}\right)^{N_\eta} \frac{\mathrm{d}y_2}{\mathrm{d}x} + \left(\xi'_z \frac{\partial \sigma_{yz}}{\partial \xi}\right)^{N_\eta} \approx \\ -\left(\eta'_y\right)^{N_\eta} \frac{3}{2\,\Delta\eta} f_y(\xi) - \left(\xi'_y\right)^{N_\eta} \frac{\mathrm{d}f_y}{\mathrm{d}\xi} + \rho \left(\frac{\partial^2 V}{\partial t^2}\right)^{N_\eta}; \\ \\ \left(\frac{\partial \sigma_{zx}}{\partial x}\right)^{N_\eta} + \left(\eta'_x \frac{\partial \sigma_{zx}}{\partial \eta}\right)^{N_\eta} + \left(\xi'_x \frac{\partial \sigma_{zx}}{\partial \xi}\right)^{N_\eta} + \left(\eta'_y\right)^{N_\eta} \frac{1}{2\,\Delta\eta} \sigma_{zy}^{N_\eta-2} - \\ \left(\eta'_y\right)^{N_\eta} \frac{4}{2\,\Delta\eta} \sigma_{zy}^{N_\eta-1} + \left(\eta'_y\right)^{N_\eta} \frac{3}{2\,\Delta\eta} \sigma_{zx}^{N_\eta} \frac{\mathrm{d}y_2}{\mathrm{d}x} + \left(\xi'_y \frac{\partial \sigma_{zx}}{\partial \xi}\right)^{N_\eta} \frac{\mathrm{d}y_2}{\mathrm{d}x} + \left(\xi'_z \frac{\partial \sigma_{zz}}{\partial \xi}\right)^{N_\eta} \approx \\ \rho g + \rho \left(\frac{\partial^2 W}{\partial t^2}\right)^{N_\eta}, \end{cases} \tag{B5}$$

where indices, "$N_\eta - 2$", "$N_\eta - 1$", and "N_η", denote respectively the numbers of the grid layers, moving from $N_\eta - 2$ in the horizontal transverse direction and ending at the ice lateral edge $y = y_2(x)$; and

$$f_x = \begin{cases} 0, \ \xi < \frac{h_\mathrm{s}}{H}; \\ -\rho_\mathrm{w} g \left(h_\mathrm{s} - \xi H\right) \frac{\mathrm{d}y_2}{\mathrm{d}x}, \ \xi \geq \frac{h_\mathrm{s}}{H}. \end{cases} \quad f_y = \begin{cases} 0, \ \xi < \frac{h_\mathrm{s}}{H}; \\ \rho_\mathrm{w} g \left(h_\mathrm{s} - \xi H\right), \ \xi \geq \frac{h_\mathrm{s}}{H}. \end{cases} \tag{B6}$$

ESDD
6, 1605–1633, 2015

The eigenvalue problem for ice-shelf vibrations

Y. V. Konovalov

References

Bassis, J. N., Fricker, H. A., Coleman, R., and Minster, J.-B.: An investigation into the forces that drive ice-shelf rift propagation on the Amery Ice Shelf, East Antarcyica, J. Glaciol., 54, 17–27, 2008.

Bromirski, P. D., Sergienko, O. V., and MacAyeal, D. R.: Transoceanic infragravity waves impacting Antarctic ice shelves, Geophys. Res. Lett., 37, L02502, doi:10.1029/2009GL041488, 2009.

Goodman, D. J., Wadhams, P., and Squire, V. A.: The flexural response of a tabular ice island to ocean swell, Ann. Glaciol., 1, 23–27, 1980.

Gudmundsson, G. H.: Ice-stream response to ocean tides and the form of the basal sliding law, The Cryosphere, 5, 259–270, doi:10.5194/tc-5-259-2011, 2011.

Holdsworth, G.: Tidal interaction with ice shelves, Ann. Geophys., 33, 133–146, 1977, http://www.ann-geophys.net/33/133/1977/.

Holdsworth, G. and Glynn, J.: Iceberg calving from floating glaciers by a vibrating mechanism, Nature, 274, 464–466, 1978.

Hughes, T. J.: West Antarctic ice streams, Rev. Geophys. Space Phys., 15, 1–46, 1977

Konovalov, Y. V.: Inversion for basal friction coefficients with a two-dimensional flow line model using Tikhonov regularization, Res. Geophys., 2, 82–89, 2012.

Konovalov, Y. V.: Ice-shelf resonance deflections modelled with a 2-D elastic centre-line model, Phys. Rev. Res. Int., 4, 9–29, 2014.

Lamb, H.: Hydrodynamics, 6th edn., Cambridge University Press, Cambridge, 1994.

Landau, L. D. and Lifshitz, E. M.: Theory of Elasticity, Vol. 7., 3rd edn., Butterworth-Heinemann, Oxford, 1986.

Lingle, C. S., Hughes T. J., and Kollmeyer, R. C.: Tidal flexure of Jakobshavns Glacier, West Greenland, J. Geophys. Res., 86, 3960–3968, 1981.

Lurie, A. I.: Theory of Elasticity, Foundations of Engineering Mechanics, Springer, Berlin, 2005.

MacAyeal, D. R., Okal, E. A., Aster, R. C., Bassis, J. N., Brunt, K. M., Cathles, L. M., Drucker, R., Fricker, H. A., Kim, Y.-J., Martin, S., Okal, M. H., Sergienko, O. V., Sponsler, M. P., and Thom, J. E.: Transoceanic wave propagation links iceberg calving margins of Antarctica with storms in tropics and Northern Hemisphere, Geophys. Res. Lett., 33, L17502, doi:10.1029/2006GL027235, 2006.

Meylan, M., Squire, V. A., and Fox, C.: Towards realism in modelling ocean wave behavior in marginal ice zones, J. Geophys. Res., 102, 22981–22991, 1997.

Reeh, N., Christensen, E. L., Mayer, C., and Olesen, O. B.: Tidal bending of glaciers: a linear viscoelastic approach, Ann. Glaciol., 37, 83–89, 2003.

Rosier, S. H. R., Gudmundsson, G. H., and Green, J. A. M.: Insights into ice stream dynamics through modelling their response to tidal forcing, The Cryosphere, 8, 1763–1775, doi:10.5194/tc-8-1763-2014, 2014.

Schmeltz, M., Rignot, E., and MacAyeal, D. R.: Tidal flexure along ice-sheets margins: comparison of InSAR with an elastic plate model, Ann. Glaciol., 34, 202–208, 2001.

Schulson, E. M.: The structure and mechanical behavior of ice, JOM-US, 51, 21–27, 1999.

Sergienko, O. V.: Elastic response of floating glacier ice to impact of long-period ocean waves, J. Geophys. Res., 115, F04028, doi:10.1029/2010JF001721, 2010.

Smith, A. M.: The use of tiltmeters to study the dynamics of Antarctic ice shelf grounding lines, J. Glaciol., 37, 51–58, 1991.

Squire, V. A., Dugan, J. P., Wadhams, P., Rottier, P. J., and Liu, A. K.: Of ocean waves and sea ice, Annu. Rev. Fluid Mech., 27, 115–168, 1995.

Turcotte, D. L. and Schubert, G.: Geodynamics, 3rd edn., Cambridge University Press, Cambridge, 2002.

Vaughan, D. G.: Tidal flexure at ice shelf margins, J. Geophys. Res., 100, 6213–6224, 2002.

Wadhams, P.: The seasonal ice zone, in: Geophysics of Sea Ice, edited by: Untersteiner, N., Plenum Press, London, 825–991, 1986.

Walker, R. T., Parizek, B. R., Alley, R. B., Anandakrishnan, S., Riverman, K. L., and Christianson, K.: Ice-shelf tidal flexure and subglacial pressure variations, Earth Planet. Sci. Lett., 361, 422–428, 2013.

ESDD

6, 1605–1633, 2015

The eigenvalue problem for ice-shelf vibrations

Y. V. Konovalov

Table 1. Eigenvalue difference due to cavity geometry changes and due to ice-shelf geometry changes in the full model.

Eigenvalue	T_1	T_2	T_3
Experiment A	37.1	14.2	7.1
Experiment B	43.2	16.8	8.4
Experiment C	66.9	21.2	10.3
Deviation (B vs. A)	15 %	17 %	17 %
Deviation (C vs. A)	57 %	40 %	37 %

ESDD
6, 1605–1633, 2015

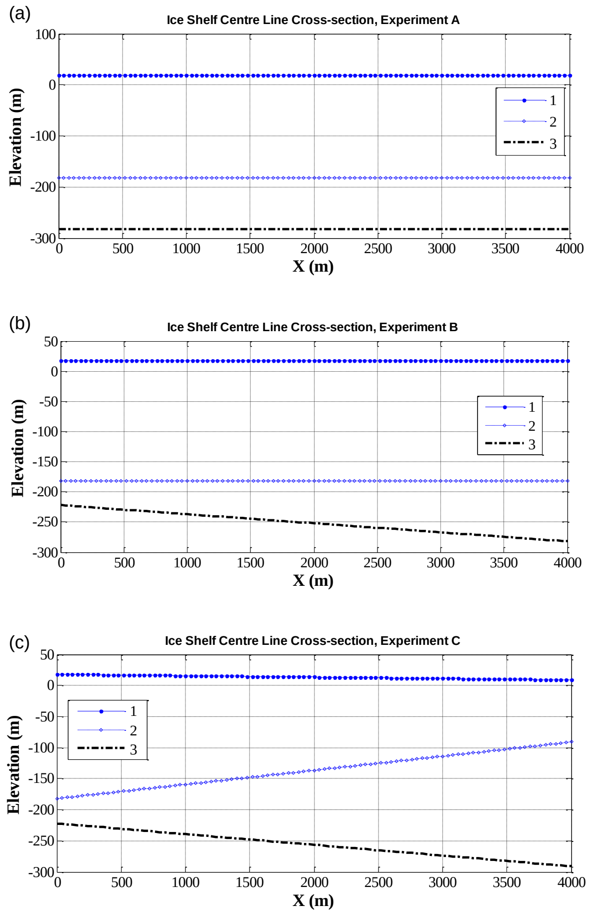

Figure 1. The ice-shelf and the cavity geometries that are considered in the three numerical experiments (A, B, C), respectively: **(a)** – ice-shelf surface, **(b)** – ice-shelf base, **(c)** – sea bottom.

ESDD
6, 1605–1633, 2015

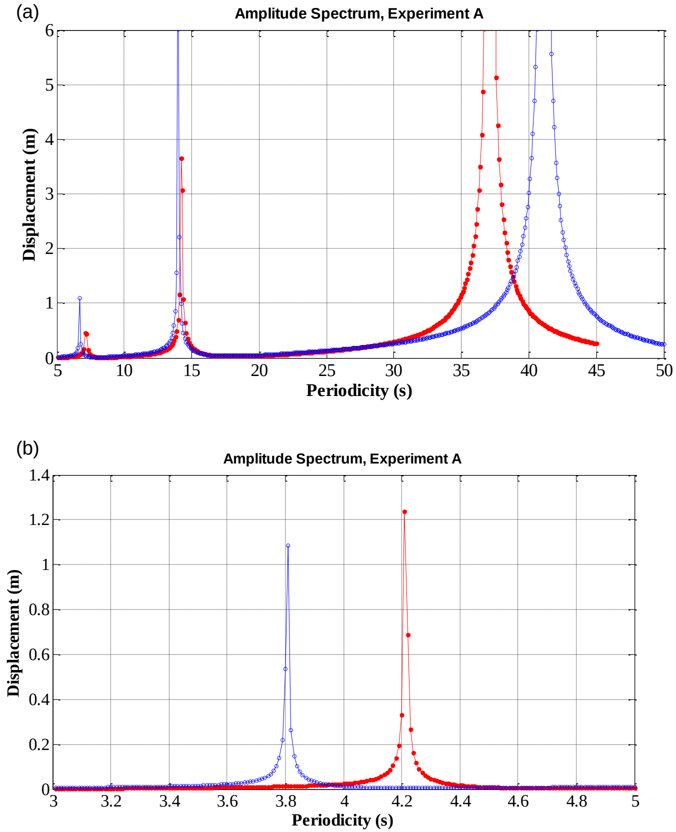

Figure 2. The amplitude spectra, maximal ice-shelf deformation vs. ocean wave periodicity, obtained in Experiment A (Fig. 1a). The red curve is the amplitude spectrum derived from the full model. The blue curve is the amplitude spectrum obtained by the Holdsworth and Glynn model. The amplitude spectra are obtained at different temporal resolutions: **(a)** temporal resolution is equal to 0.1 s for periodicity varying in the range of 5 to 50 s; **(b)** temporal resolution is equal to 0.01 s for periodicity in the range of 3 to 5 s.

ESDD
6, 1605–1633, 2015

The eigenvalue problem for ice-shelf vibrations

Y. V. Konovalov

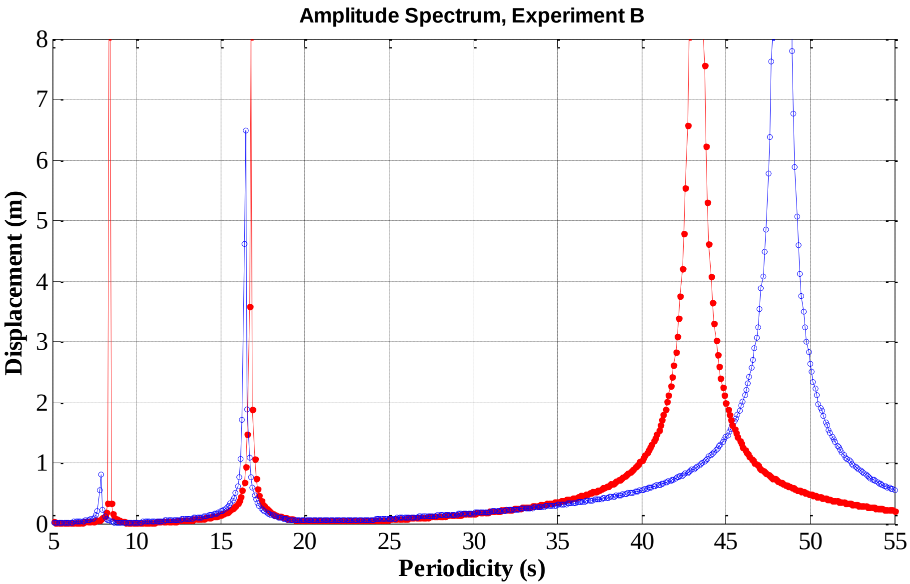

Figure 3. The amplitude spectra obtained in Experiment B (Fig. 1b). The red curve is the amplitude spectrum obtained by the full model. The blue curve is the amplitude spectrum obtained by the Holdsworth and Glynn model.

ESDD
6, 1605–1633, 2015

The eigenvalue problem for ice-shelf vibrations

Y. V. Konovalov

Title Page
Abstract | Introduction
Conclusions | References
Tables | Figures
◀I | ▶I
◀ | ▶
Back | Close
Full Screen / Esc
Printer-friendly Version
Interactive Discussion

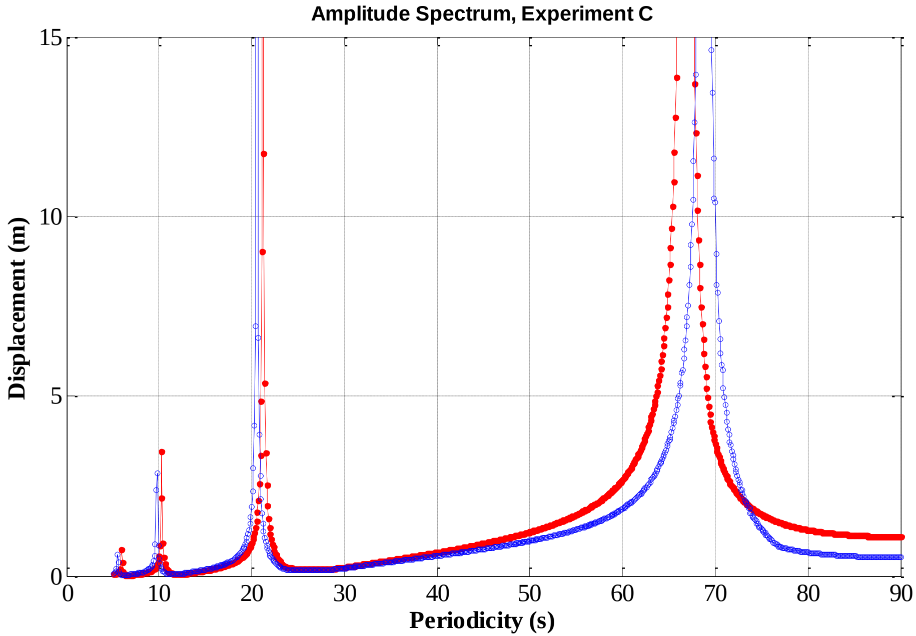

Figure 4. The amplitude spectra obtained in Experiment C (Fig. 1c). The red curve is the amplitude spectrum obtained by the full model. The blue curve is the amplitude spectrum obtained by the Holdsworth and Glynn model. The temporal resolution is equal to 0.1 s.

ESDD
6, 1605–1633, 2015

The eigenvalue problem for ice-shelf vibrations

Y. V. Konovalov

ESDD
6, 1605–1633, 2015

The eigenvalue problem for ice-shelf vibrations

Y. V. Konovalov

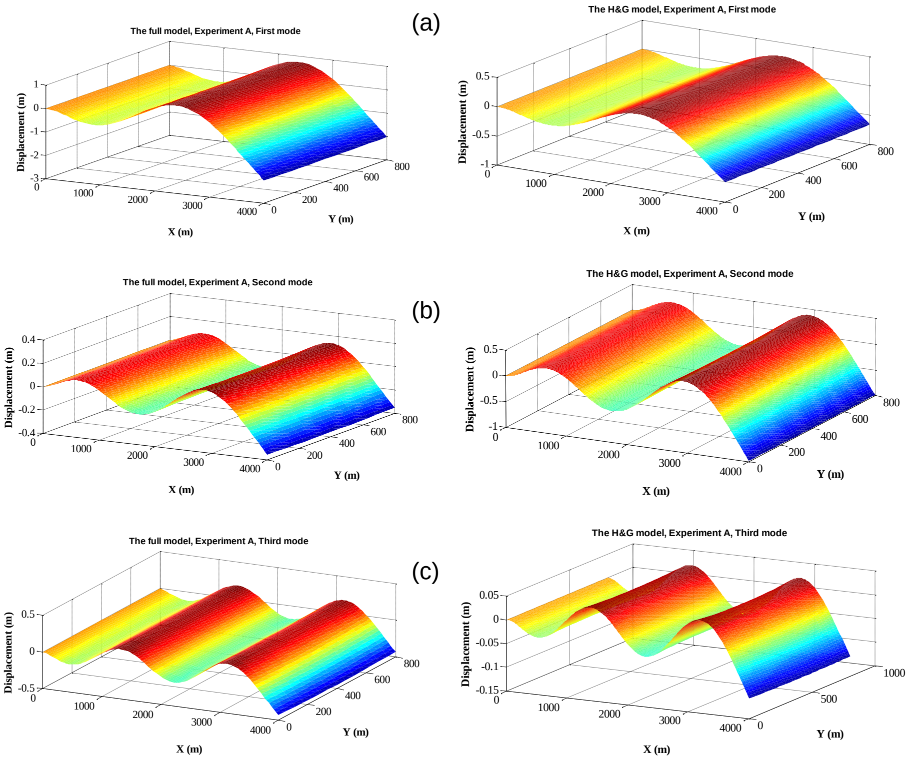

Figure 5. Ice-shelf deformations obtained for the first three modes in Experiment A. The plots on the left show the deformations obtained by the full model. The plots on the right show the deformations obtained by the Holdsworth and Glynn model. **(a)** The periodicities are equal to 37.1 s and 41.1 s, respectively; **(b)** the periodicities are equal to 14.2 s and 14 s, respectively; **(c)** the periodicities are equal to 7.1 s and 6.7 s, respectively. Young's modulus $E = 9$ GPa; Poisson's ratio $\nu = 0.33$ (Schulson, 1999).

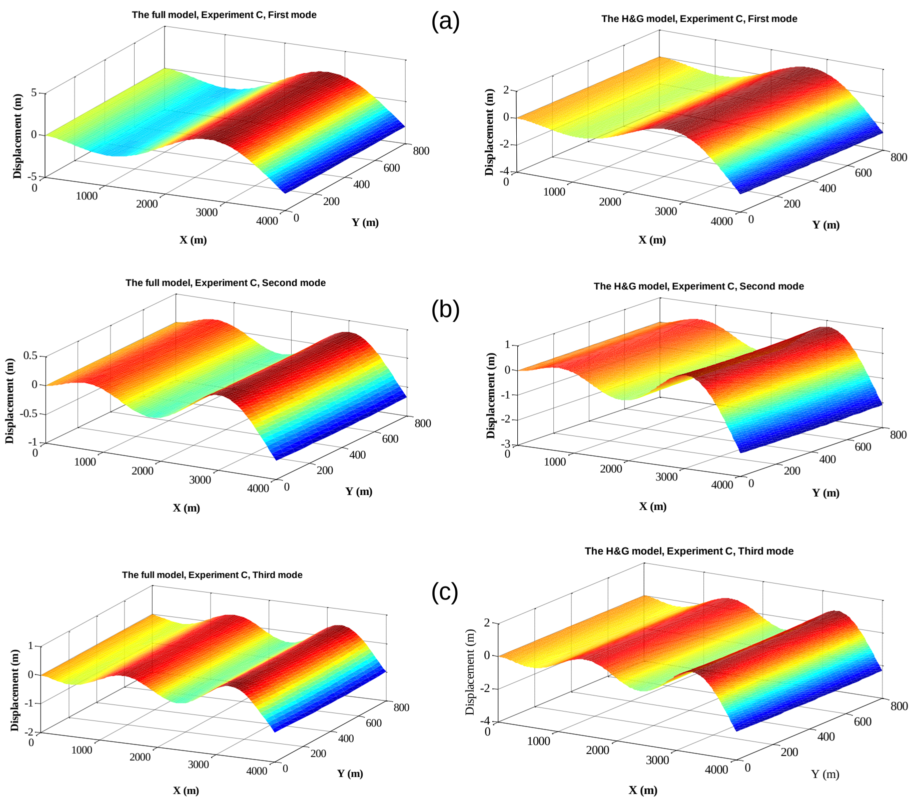

Figure 6. Ice-shelf deformations obtained in Experiment C. The plots on the left show the deformations obtained by the full model for the first, second and third modes. The plots on the right show the deformations obtained by the Holdsworth and Glynn model for the first three modes. **(a)** The periodicities are equal to 66.9 s and 68.8 s, respectively; **(b)** the periodicities are equal to 21.2 s and 20.5 s, respectively; **(c)** the periodicities are equal to 10.3 s and 9.8 s, respectively. Young's modulus $E = 9$ GPa; Poisson's ratio $\nu = 0.33$ (Schulson, 1999).

ESDD
6, 1605–1633, 2015

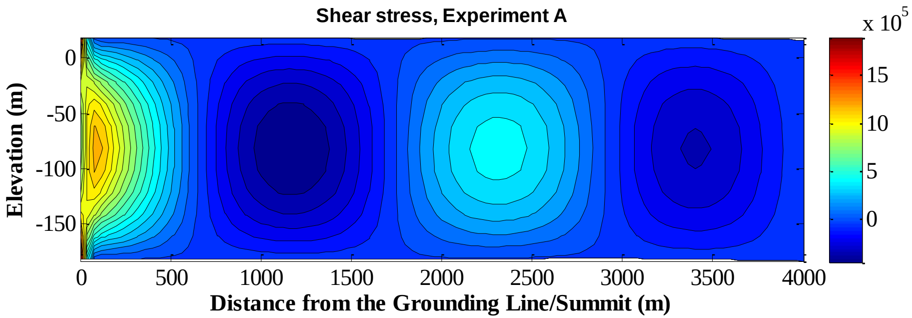

Figure 7. Shear stress distribution in the vertical cross-section along the centre line. The distributions are obtained in Experiment A for the second mode. The incident wave amplitude is equal to 0.5 m.

ESDD
6, 1605–1633, 2015

The eigenvalue problem for ice-shelf vibrations

Y. V. Konovalov